Available online at www.sciencedirect.com

ScienceDirect

Green Energy & Environment 5 (2020) 76–82

www.keaipublishing.com/gee

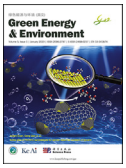

Research paper

Active sites of Pt/CNTs nanocatalysts for aerobic base-free oxidation of glycerol

Minjian Pan [a], Jingnan Wang [a], Wenzhao Fu [a], Bingxu Chen [a], Jiaqi Lei [a], Wenyao Chen [a], Xuezhi Duan [a,*], De Chen [b], Gang Qian [a,*], Xinggui Zhou [a]

[a] State Key Laboratory of Chemical Engineering, East China University of Science and Technology, 130 Meilong Road, Shanghai, 200237, China
[b] Department of Chemical Engineering, Norwegian University of Science and Technology, Trondheim, 7491, Norway

Received 10 January 2019; revised 19 July 2019; accepted 8 August 2019
Available online 8 September 2019

Abstract

Understanding the nature of Pt active sites is of great importance for the structure-sensitive base-free oxidation of glycerol. In the present work, the remarkable Pt particle size effects on glycerol conversion and products formation from the oxidation of the primary and the secondary hydroxyl groups are understood by combining the model calculations and DFT calculations, aiming to discriminate the corresponding dominant Pt active sites. The Pt(100) facet is demonstrated to be the dominant active sites for the glycerol conversion and the products formation from the two routes. The insights revealed here could shed new light on fundamental understanding of the Pt particle size effects and then guiding the design and optimization of Pt-catalyzed base-free oxidation of glycerol toward targeted products.

Keywords: Base-free oxidation of glycerol; Pt/CNTs catalyst; Active sites; Model calculations; DFT calculations

1. Introduction

The aerobic base-free oxidation of glycerol over supported platinum catalysts affords a simple, sustainable and environmentally benign route to produce various value-added fine chemicals yet to suppress occurrence of C–C cleavage side reactions [1–7]. Typically, this process is highly sensitive to not only the Pt electronic properties [8,9], but also the Pt particle size [7,10,11], which is a so-called structure-sensitive reaction. Recently, an optimal Pt particle size (i.e., ~2.5 nm) was observed for the reaction over differently sized Pt nanoparticles supported on carbon nanotubes (CNTs) catalysts [7]. Our previous studies showed that the differently sized Pt/CNTs catalysts we used have similar Pt electronic properties [12,13]. Thus, their different catalytic activities in principle arise from the difference in the fraction and number of Pt active sites. An attempt is therefore highly desirable to discriminate and then understand the dominant Pt active sites for the reaction.

Multiple techniques, including well-defined catalyst preparation, surface science studies and model/ab-initio calculations, increasingly facilitate the understanding of the nature of active sites [13–21]. Among them, we have developed a new method based on the model calculations in our previous work to reveal the nature of the metal particle size effects and then discriminate the dominant active sites using the hydrolytic dehydrogenation of ammonia borane with almost no selectivity issues as the probe reaction [13]. As a consecutive effort, we employ this method for the full exploration of the structure-sensitive Pt/CNTs catalyzed base-free oxidation of glycerol with selectivity issues. As schematically shown in Scheme 1, the oxidation of the primary hydroxyl group of

* Corresponding authors.
E-mail addresses: xzduan@ecust.edu.cn (X. Duan), carlqg@ecust.edu.cn (G. Qian).

https://doi.org/10.1016/j.gee.2019.08.001

glycerol, i.e., Route I, mainly generates glyceraldehyde (GLYD) and glyceric acid (GLYA), while that of the secondary one, i.e., Route II, mainly yields dihydroxyacetone (DHA). This calls for a better understanding of the dominant active sites for products formation from the two routes, aiming to guide the design of highly efficient Pt catalysts.

The objective of this work is to discriminate the dominant Pt active sites for the glycerol conversion as well as products formation from Route I and Route II. Model calculations were employed to estimate the numbers of corner, edge, (111), (100) and interface atoms over differently sized Pt/CNTs catalysts on the basis of their shape characterized by HRTEM. Then, the $TOF_{active\ site}$ for the glycerol conversion and products formation from the two routes based on each exposed crystal facets/sites was plotted with the Pt particle size to determine which specific sites mainly dominate the activity and selectivity, respectively. Moreover, the adsorption behaviors of glycerol and the activation of its primary and secondary hydroxyl groups on the two typical Pt(111) and Pt(100) surfaces were comparatively investigated using DFT calculations to reveal the nature of Pt active sites.

2. Experimental

In our previous work, the differently sized Pt/CNTs catalysts prepared by incipient wetness impregnation method have been employed to catalyze the base-free oxidation of glycerol, and the size-dependent glycerol conversion and products selectivity have been revealed [7]. As a consecutive effort, in this work, we employ our proposed method to discriminate the dominant Pt active sites for the glycerol conversion as well as products formation from Route I and Route II. The initial rates of the glycerol conversion and products formation from the two routes were calculated from the data of our previous work [7], respectively, and the shapes of Pt nanoparticles supported on CNTs were characterized by high resolution transmission electron microscopy (HRTEM, JEOL JEM-2100F, Japan).

DFT calculations were further performed using the Vienna Ab-initio Simulation Package (VASP) [22–24] to reveal the nature of Pt active sites for the selective oxidation of glycerol. The solution of the Kohn-Sham equations was expanded in a plane wave basis set with a cutoff energy of 400 eV. The interaction between valence electrons and ion cores was treated by the PAW method [25,26]. The correlation and exchange energies were obtained using the Perdew–Burke–Ernzerhof (PBE) generalized gradient approximation (GGA) functional [27,28]. The Brillouin zone sampling was performed using a Monkhorst–Pack grid, and the electronic occupancies were determined in light of a Methfessel-Paxton scheme with an energy smearing of 0.2 eV. A relaxation was performed until the maximum force upon each atom (maximum force, as it will be referred to) was less than 0.03 eV $Å^{-1}$, and the wave functions were converged to within 10^{-6} eV.

We obtained a DFT-determined equilibrium lattice constant of 3.98 Å for bulk Pt in the face-centered-cubic (fcc) structure, which is in good agreement with the experimental bulk lattice constant (3.92 Å) [29] and the theoretically calculated bulk lattice constants reported in previous work [30]. A supercell lattice of 4 × 4 was chosen in order to accommodate the reacting species with minimal interaction between supercells. For the calculation of surfaces, glycerol adsorption and transition state for dehydrogenation step, the bottom two-layered Pt were fixed, while the top two-layered Pt as well as the adsorbates were relaxed. The Monkhorst–Pack mesh of 3 × 3 × 1 k-point sampling in the surface Brillouin zone was used. To minimize the interactions between the slabs, we employed a vacuum gap spacing of 12 Å.

The dimer method was used to determine the transition states of the elementary steps of glycerol dehydrogenation via the O–H bond cleavage [31]. In all the calculations, a force-based conjugated gradient method was used to optimize the geometries [32]. The vibrational frequencies were analyzed to evaluate if a stationary point is a minimum state with no imaginary frequencies or a transition state with only one imaginary frequency. Moreover, the zero-point energy (ZPE) was taken into account for all the calculated energy data unless otherwise stated.

The adsorption energy (E_{ads}) and the activation barrier (E_a) were determined by Eqs. (1) and (2), respectively:

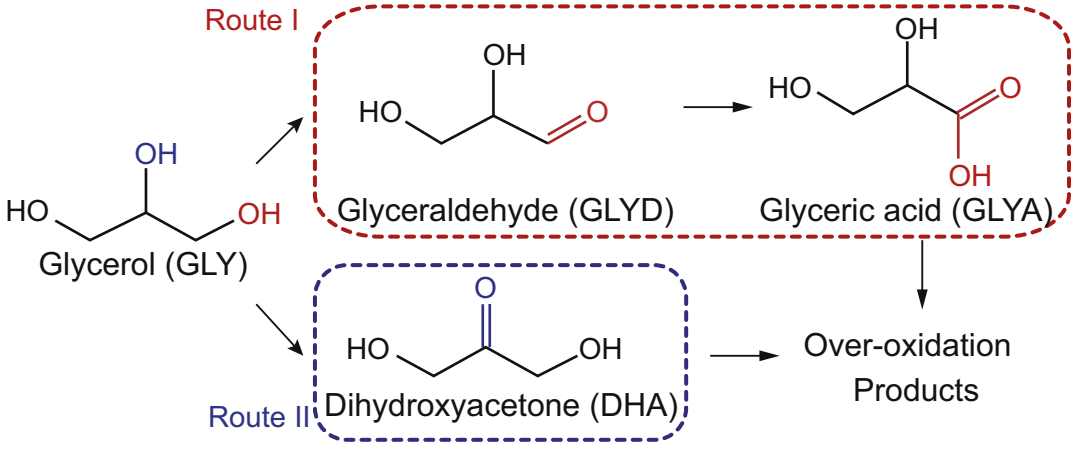

Scheme 1. Main reaction routes for glycerol oxidation over the Pt-based catalysts.

$$E_{ads} = E_{GLY/slab} - E_{GLY} - E_{slab} \quad (1)$$

$$E_a = E_{TS} - E_{IS} \quad (2)$$

where $E_{GLY/slab}$, E_{GLY}, E_{slab}, E_{TS} and E_{IS} are the energies of slab with glycerol on the surface, glycerol in gas phase, the slab of clean surface, the transition state (TS) and the most stable initial state (IS), respectively.

3. Results and discussion

3.1. Discrimination of dominant Pt active sites

As described in the Introduction, the base-free oxidation of glycerol over Pt-based catalysts is a well-known structure-sensitive reaction [7,10,11]. Understanding the origin of the size effects is highly desirable to optimize the catalyst performance. In our previous work [13], we have developed a method based on the model calculations to reveal the nature of the metal particle size effects and then discriminate the dominant active sites. Along this line, this method is used to discriminate the dominant Pt active sites for the glycerol conversion and products formation.

Considering that not all the exposed surface atoms can act as the active sites, the size-dependent initial reaction rates and products formation rates rather than the apparent turnover frequency (TOF) are calculated here from the data of our previous work shown in Fig. 1a [7], because the calculation of intrinsic TOF is based on the number of active sites. Taking glycerol conversion over 5 wt% Pt/CNTs catalyst with an average Pt particle size of 2.5 nm as an example, the initial glycerol conversion rate ($r_{initial}$) can be calculated from the slope of the curve by extrapolation to zero time, as illustrated in Fig. 1b. Similarly, the initial formation rates of the products from the oxidation of the primary hydroxyl groups (GLYD and GLYA) and that of the secondary one (DHA) can be also determined, respectively. The obtained initial glycerol conversion rates and product formation rates are correlated with the average Pt particle size, as shown in Fig. 1c. The size-dependent activity and selectivity can be observed, the origin of which will be revealed using our proposed method as follows.

In order to calculate the intrinsic TOF, the number of active sites should be firstly determined. Although CO absorption is a very useful tool to measure the number of exposed surface atoms, it cannot determine the number of different active sites, such as (100) and (111) sites. Therefore, in this work, the model calculations method is used to determine the number of different active sites and then calculate the corresponding $TOF_{active\ site}$. For the model calculations method [13], it is based on the assumptions that only one specific active site dominates the reaction, and the activity of such specific active site is uniform regardless of the Pt particle size when these differently sized Pt catalysts exhibit similar electronic properties, i.e., there are no Pt electronic effects. Then, the $r_{initial}$ of the catalysts would increase linearly with the number of such specific Pt active sites, and thus the $TOF_{active\ site}$ based on the number of such specific active sites should be constant. In other words, there exists independence of the $TOF_{active\ site}$ on the Pt particle size. Considering different $TOF_{active\ site}$ based on the number of each exposed crystal facets/sites, the normalized TOF is used for clear comparison, which is defined as the ratio of each TOF point to the highest TOF for each exposed crystal facets/sites. Therefore, by plotting the normalized $TOF_{active\ site}$ with the metal particle size, we can determine which specific exposed crystal facets/sites give rise to an almost size-independent trend, that is, this typed active sites mainly dominate the reaction. The procedure for the model calculations is schematically shown in Fig. S1, and the details of how the normalized TOFs derived are also illustrated in the supporting information.

To figure out which type of site is the dominant active site, it is necessary to firstly determine the variation in the number of each type of sites with Pt particle size, which is highly dependent on the morphology of Pt particles. HRTEM was employed to characterize the shape of Pt particles supported on CNTs. The typical HRTEM image and its corresponding fast Fourier transform pattern of Pt nanoparticle are shown in Fig. 2a. The Pt(111) and Pt(200) are detected, which are in consistent with previous observations [33,34]. Considering

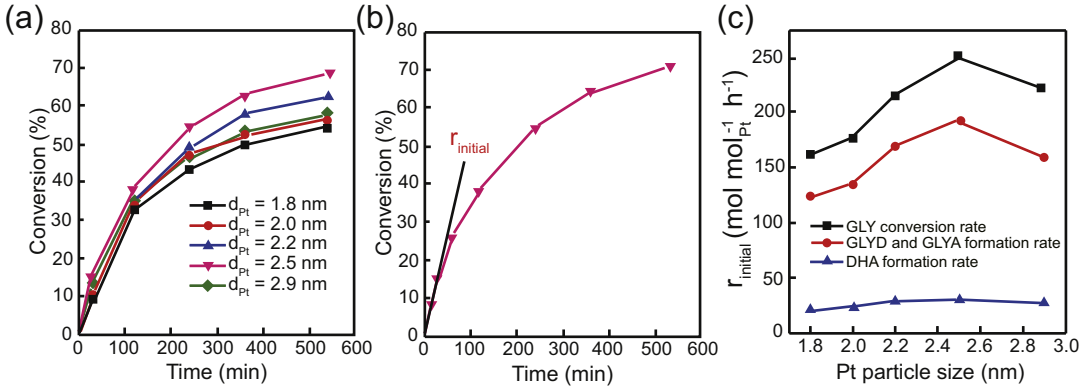

Fig. 1. (a) Glycerol conversion as a function of time over differently sized Pt/CNTs catalysts [7]. (b) Scheme of $r_{initial}$ calculation from the slope of the curve by extrapolation to zero time by taking 5 wt% Pt/CNTs catalyst as an example. (c) $r_{initial}$ of glycerol conversion (black points), GLYD and GLYA formation (red points) and DHA formation (blue points) as a function of Pt particle size.

that the Pt(200) and Pt(100) planes are equivalent and parallel ones and the interplanar spacing of the Pt(100) is twice that of the Pt(200), the Pt(100) was used for the following calculations.

The shape of Pt nanoparticle can be best represented by half truncated cuboctahedron with the top facet of (100), as schematically shown in Fig. 2b. Considering the truncated cuboctahedron is symmetric, it is reasonable to use the formulas in Table S1 [35] to calculate the numbers of (100), (111), edge, corner or interface atoms per mole of Pt for the differently sized Pt/CNTs catalysts with half truncated cuboctahedron, and the results are shown in Fig. 2c. By combining all the above data, the normalized $TOF_{active\ site}$ as a function of Pt particle size for glycerol conversion and products formation from the two routes based on each exposed crystal facets/sites can be obtained, and the results are shown in Fig. 2d. It can be seen that the normalized TOFs are highly dependent on Pt particle size when the (111) facet atoms, the edge atoms, the corner atoms or interface atoms are respectively considered as the active sites. However, it should be noted that when the (100) facet atoms are considered as the active sites, the normalized TOFs for the glycerol conversion and products formation from the two routes have a weak dependence on Pt particle size. These results suggest that the (100) facet atoms of Pt/CNTs catalysts may be the dominant active sites for the glycerol conversion.

Moreover, Fig. 2d also suggests that the (100) facet atoms are the dominant active sites for products formation from the oxidation of both the primary and the secondary hydroxyl groups. In other words, the dominant active sites for products

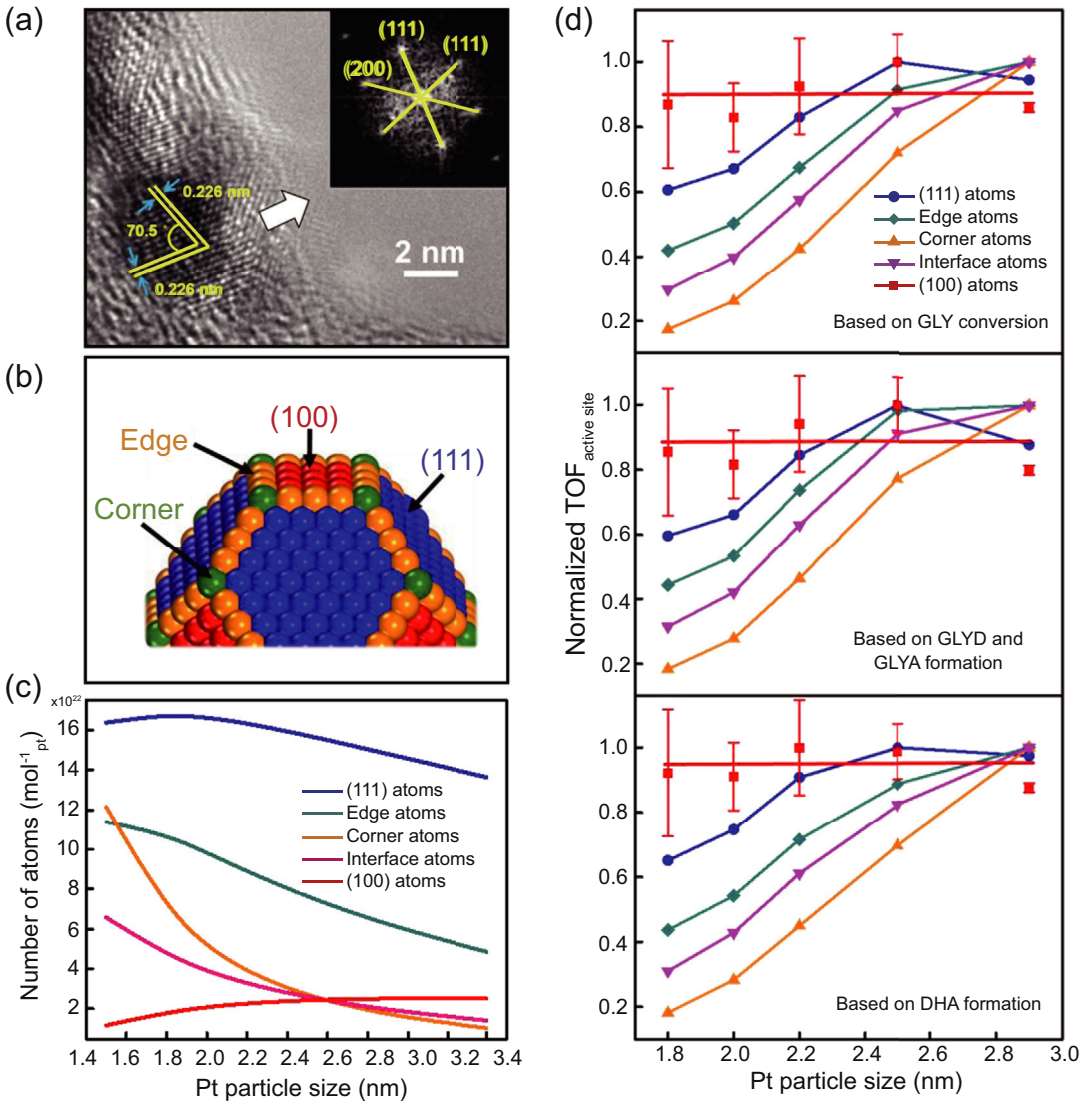

Fig. 2. (a) Typical HRTEM image of Pt nanoparticle supported on CNTs, the inset is the corresponding fast Fourier transform pattern. (b) Schematic diagram of truncated cuboctahedron. (c) Plots of number of surface atoms per mole of Pt with Pt particle size. (d) Plots of normalized $TOF_{active\ site}$ based on GLY conversion, GLYD and GLYA formation, and DHA formation with Pt particle size. The error bars represent the standard deviations of the normalized TOFs originated from the standard deviations of the Pt particle sizes listed in Table S2. For clarity, the error bar is only shown there for the (100) plane, and other error bars are shown in Fig. S2.

formation from the two routes are similar. Additonally, our previous studies have shown that for the Pt/CNTs catalysts with particle size larger than 1.8 nm, they possess similar electronic properties [13]. Therefore, the origin of the size-dependent initial conversion rate of glycerol and formation rates of the products from the two routes can be inferred to mainly arise from the difference in the number of Pt active sites, i.e., the Pt geometric properties.

3.2. Theoretical understanding of the nature of Pt active sites

To reveal the nature of Pt active sites for the selective oxidation of glycerol, we resort to DFT calculations toward an atomic-level understanding. The glycerol adsorption and activation were calculated on two typical Pt terraced surfaces, i.e., the closed-packed Pt(111) surface and the more open Pt(100) surface, where the Pt stepped surfaces are not included, because these surfaces are easily blocked by strongly adsorbed species in alcohol oxidation reactions [36]. Fig. 3 shows the most stable adsorption configurations, adsorption energies and O–H bond lengths of glycerol on the Pt(111) and the Pt(100) surfaces via the oxygen atom in its primary or secondary hydroxyl group. Clearly, the glycerol adsorption via the oxygen atom in its primary hydroxyl group, especially for the Pt(100) surface, is stronger than that in its secondary hydroxyl group. In addition, Fig. 3a and b show that the bond length of O–H in the primary hydroxyl group increases from 0.976 Å to 0.981 Å and 0.982 Å on the Pt(111) and Pt(100) surfaces, respectively, and Fig. 3c and d illustrate the bond length of O–H in the secondary hydroxyl group increasing from 0.978 Å to 0.994 Å and 0.997 Å on the Pt(111) and Pt(100) surfaces, respectively. These larger elongations of O–H bonds in the primary and secondary hydroxyl groups on the Pt(100) surface suggest the preferential activation of glycerol on such surface.

According to previous studies showing that the alcohol dehydrogenation starts from the O–H bond cleavage [37], the activation behaviors of glycerol via the O–H bond cleavage on the Pt(111) and the Pt(100) surfaces were comparatively studied. The identified transition states configurations are shown in Fig. S3, and the energy profiles are plotted in Fig. 4. Obviously, the Pt(100) surface shows lower activation barrier for the O–H bond cleavage in both the primary and secondary hydroxyl groups than the Pt(111) surface. Meanwhile, the O–H bond cleavage is exothermic on the Pt(100) surface, while that is endothermic on the Pt(111) surface. These results strongly indicate the preferential occurrence of the O–H bond cleavage on the Pt(100) surface. In other words, the Pt(100) surface most likely acts as the active sites for the glycerol conversion.

3.3. General discussion

As demonstrated above, the Pt(100) surface is discriminated as dominant active sites for the reaction based on the model calculations method, which is valuable for the rational design and optimization of Pt catalysts by tailoring the fraction of Pt(100) with the aid of surface-stabilizing reagent [38] or foreign metal ions [39]. This is consistent with the experimental results of the significantly higher activities with cuboctahedral Pt nanoparticles primarily exposing (100) surface, in comparison with the performance of tetrahedral samples exposing (111) surface [40]. Moreover, for the

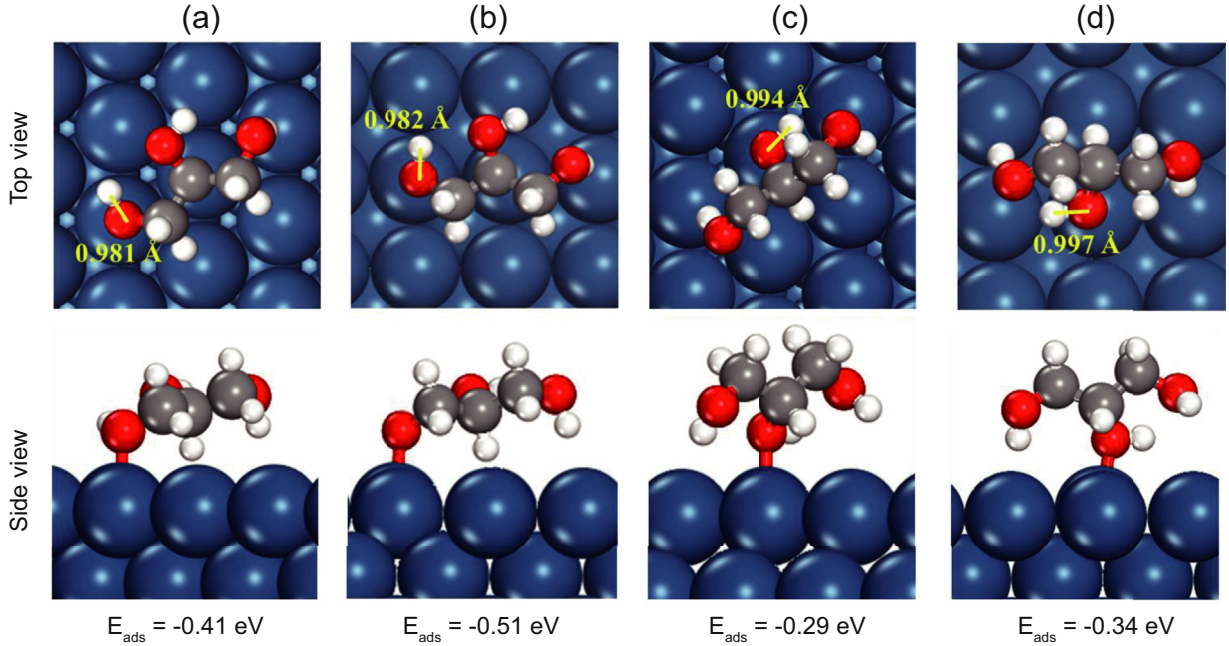

Fig. 3. The most stable adsorption configurations, adsorption energies and O–H bond lengths of glycerol on the Pt(111) (a and c) and the Pt(100) (b and d) surfaces via the oxygen atom in its primary or secondary hydroxyl group. Gray, red, white and blue balls represent C, O, H and Pt atoms, respectively.

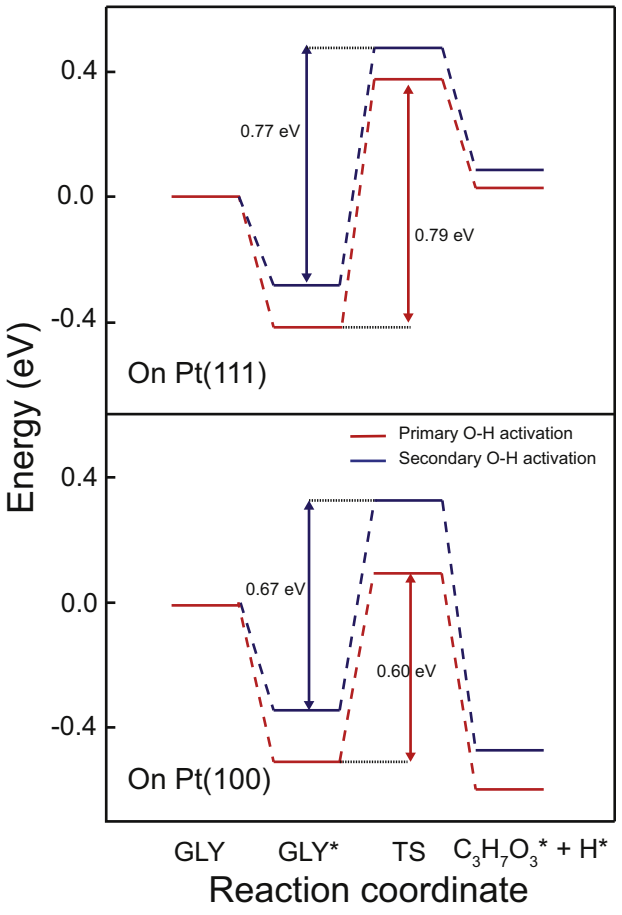

Fig. 4. Energy profiles for the dehydrogenation of the primary and secondary hydroxyl groups of glycerol on the Pt(111) and the Pt(100) surfaces.

oxidation of primary and secondary hydroxyl groups, their active sites are observed to be the same surface, i.e., the Pt(100) surface. However, on such surface, the adsorption stability of glycerol via the oxygen atom in the primary hydroxyl group is stronger, and the corresponding O–H bond cleavage barrier is lower, which suggests a higher reaction rate for the primary hydroxyl group oxidation. This can provide an interpretation for the results shown in Fig. 1c, i.e., higher GLYD and GLYA formation rate compared to DHA formation rate.

Our previous DFT calculations and kinetic isotopic studies showed that the Pt(111) surface is dominant active sites for oxygen dissociation by water-assited oxygen activation [41], and the oxygen activation steps are in equilibrium rather in rate determining step [42]. The activated oxygen species, i.e., OH*, most likely diffuses from the Pt(111) to the Pt(100) acting as the dominant active sites for glycerol conversion. It is noted that the studies on the OH* assisted glycerol conversion have not yet been included in this work, and the studies on this challenging issue is still ongoing in our group.

Further combining previous studies, it is suggested that tailoring the Pt electronic properties by changing the catalyst preparation method [8] or introducing heteroatoms to the support [43] can tune the activity of glycerol conversion. Moreover, the addition of second metal to Pt has been revealed to modify the product selectivity. For example, the Sb or Bi promoted Pt catalysts are more favorable for the preferential oxidation of the secondary hydroxyl group to form DHA [34,44], while the Cu or Co promoted Pt catalysts are more favorable for the preferential oxidation of the primary hydroxyl group to form GLYA [11,45]. In our recent studies, we have employed DFT calculations to investigate the adsorption configurations of glycerol on clean Pt surface and SbO adsorbed Pt surface, and found that the preferential adsorption configuration of glycerol has been changed from the primary to secondary hydroxyl group in the presence of promoter [10]. All these are very interesting subjects, whose mechanistic understanding is highly desirable to guide the rational design of Pt catalysts toward preferentially selective oxidation of glycrol to targeted products. This will be carried out in our future work.

4. Conclusions

In summary, we have successfully combined the model calculations with the DFT calculations to understand the nature of the size effects in Pt/CNTs catalyzed base-free glycerol oxidation, and then to discriminate the dominant Pt active sites for the glycerol conversion and products formation from the oxidation of the primary and the secondary hydroxyl groups. According to the almost size-insensitive $TOF_{active\ site}$, the Pt(100) facet were discriminated as the dominant active sites for glycerol conversion as well as products formation from the two routes, and the origin of the structure sensitivity mainly resulted from the difference in the Pt geometric properties. The DFT calculations further revealed the preferential occurrence of the O–H bond cleavage in both the primary and secondary hydroxyl groups on the Pt(100) surface, suggesting that the Pt(100) surface is much more active than the Pt(111) surface.

Conflict of interests

The authors declare that they have no known competing financial interests or personal relationships that could have appeared to influence the work reported in this paper.

Acknowledgments

This work was financially supported by the Natural Science Foundation of China (21776077), the Shanghai Natural Science Foundation (17ZR1407300 and 17ZR1407500), the Program for Professor of Special Appointment (Eastern Scholar) at Shanghai Institutions of Higher Learning, the Shanghai Rising-Star Program (17QA1401200), the Open Project of State Key Laboratory of Chemical Engineering (SKLChe-15C03), the State Key Laboratory of Organic–Inorganic Composites (oic-201801007), the Fundamental Research Funds for the Central Universities (222201718003), and the 111 Project of the Ministry of Education of China (B08021).

Appendix A. Supplementary data

Supplementary data to this article can be found online at https://doi.org/10.1016/j.gee.2019.08.001.

References

[1] G. Dodekatos, S. Schünemann, H. Tüysüz, ACS Catal. 8 (2018) 6301–6333.
[2] Y.Y. Sun, X.W. Li, J.G. Wang, W.S. Ning, J. Fu, X.Y. Lu, Z.Y. Hou, Appl. Catal. B Environ. 218 (2017) 538–554.
[3] M.Y. Zhang, J.J. Shi, W.S. Ning, Z.Y. Hou, Catal. Today 298 (2017) 234–240.
[4] X.M. Ning, L. Zhan, H.J. Wang, H. Yu, F. Peng, New J. Chem. 42 (2018) 18837–18843.
[5] X.M. Ning, Y.H. Li, H. Yu, F. Peng, H.J. Wang, Y.H. Yang, J. Catal. 335 (2016) 95–104.
[6] D. Motta, F.J.S. Trujillo, N. Dimitratos, A. Villa, L. Prati, Catal. Today 308 (2018) 50–57.
[7] J.Q. Lei, X.Z. Duan, G. Qian, X.G. Zhou, D. Chen, Ind. Eng. Chem. Res. 53 (2014) 16309–16315.
[8] J.Q. Lei, H. Dong, X.Z. Duan, W.Y. Chen, G. Qian, D. Chen, X.G. Zhou, Ind. Eng. Chem. Res. 55 (2016) 420–427.
[9] X.M. Ning, H. Yu, F. Peng, H.J. Wang, J. Catal. 325 (2015) 136–144.
[10] X.Z. Duan, Y.F. Zhang, M.J. Pan, H. Dong, B.X. Chen, Y.Y. Ma, G. Qian, X.G. Zhou, J. Yang, D. Chen, AIChE J. 64 (2018) 3979–3987.
[11] D. Liang, J. Gao, H. Sun, P. Chen, Z.Y. Hou, Appl. Catal. B Environ. 106 (2011) 423–432.
[12] W.Y. Chen, J. Ji, X.Z. Duan, G. Qian, P. Li, X.G. Zhou, D. Chen, W.K. Yuan, Chem. Commun. 50 (2014) 2142–2144.
[13] W.Y. Chen, J. Ji, X. Feng, X.Z. Duan, G. Qian, P. Li, X.G. Zhou, D. Chen, W.K. Yuan, J. Am. Chem. Soc. 136 (2014) 16736–16739.
[14] W.Z. Fu, W.Y. Chen, G. Qian, D. Chen, W.K. Yuan, X.G. Zhou, X.Z. Duan, React. Chem. Eng. 4 (2019) 316–322.
[15] Y. Xiao, J. Greeley, A. Varma, Z.J. Zhao, G.M. Xiao, AIChE J. 63 (2017) 705–715.
[16] Z.J. Chen, Y. Mao, J.F. Chen, H.F. Wang, Y.D. Li, P. Hu, ACS Catal. 7 (2017) 4281–4290.
[17] Z. Li, T. He, L. Liu, W.D. Chen, M. Zhang, G.T. Wu, P. Chen, Chem. Sci. 8 (2017) 781–788.
[18] J.K. Zhang, W.Y. Chen, H.B. Ge, C.Q. Chen, W.J. Yan, Z. Gao, J. Gan, B.Y. Zhang, X.Z. Duan, Y. Qin, Appl. Catal. B Environ. 235 (2018) 256–263.
[19] W.Y. Chen, Z.J. Wang, X.Z. Duan, G. Qian, D. Chen, X.G. Zhou, Chem. Eng. Sci. 192 (2018) 1242–1251.
[20] C.C. Hou, Q. Li, C.J. Wang, C.Y. Peng, Q.Q. Chen, H.F. Ye, W.F. Fu, C.M. Che, N. López, Y. Chen, Energy Environ. Sci. 10 (2017) 1770–1776.
[21] Y.Q. Cao, W.Z. Fu, Z.J. Sui, X.Z. Duan, D. Chen, X.G. Zhou, Ind. Eng. Chem. Res. 58 (2019) 1888–1895.
[22] G. Kresse, J. Furthmuller, Comput. Mater. Sci. 6 (1996) 15–50.
[23] G. Kresse, J. Hafner, Phys. Rev. B 49 (1994) 14251–14269.
[24] G. Kresse, J. Hafner, Phys. Rev. B 47 (1993) 558–561.
[25] G. Kresse, J. Furthmuller, Phys. Rev. B 54 (1996) 11169–11186.
[26] P.E. Blochl, Phys. Rev. B 50 (1994) 17953–17979.
[27] G. Kresse, D. Joubert, Phys. Rev. B 59 (1999) 1758–1775.
[28] J.P. Perdew, K. Burke, M. Ernzerhof, Phys. Rev. Lett. 77 (1996) 3865–3868.
[29] C. Kittel, Introduction to Solid State Physics, seventh ed., John Wiley & Sons, Inc., New York, 1996.
[30] P. Tereshchuk, A.S. Chaves, J.L.F. Da Silva, J. Phys. Chem. C 118 (2014) 15251–15259.
[31] G. Henkelman, H. Jonsson, J. Chem. Phys. 111 (1999) 7010–7022.
[32] D. Sheppard, R. Terrell, G. Henkelman, J. Chem. Phys. 128 (2008), 134106.
[33] M.Y. Zhang, J.J. Shi, Y.Y. Sun, W.S. Ning, Z.Y. Hou, Catal. Commun. 70 (2015) 72–76.
[34] R.F. Nie, D. Liang, L. Shen, J. Gao, P. Chen, Z.Y. Hou, Appl. Catal. B Environ. 127 (2012) 212–220.
[35] R. Van Hardeveld, F. Hartog, Sci. Sci. 15 (1969) 189–230.
[36] H.F. Wang, Z.P. Liu, J. Am. Chem. Soc. 130 (2008) 10996–11004.
[37] B.N. Zope, D.D. Hibbitts, M. Neurock, R.J. Davis, Science 330 (2010) 74–78.
[38] H. Lee, S.E. Habas, S. Kweskin, D. Butcher, G.A. Somorjai, P.D. Yang, Angew. Chem. Int. Ed. 45 (2006) 7824–7828.
[39] H. Song, F. Kim, S. Connor, G.A. Somorjai, P.D. Yang, J. Phys. Chem. B 109 (2005) 188–193.
[40] Y. Li, F. Zaera, J. Catal. 326 (2015) 116–126.
[41] J. Gan, W. Luo, W.Y. Chen, J.N. Guo, Z.H. Xiang, B.X. Chen, F. Yang, Y.J. Cao, F. Song, X.Z. Duan, X.G. Zhou, Eur. J. Inorg. Chem. 27 (2019) 3210-3217.
[42] Y.Y. Ma, J. Gan, M.J. Pan, Y.F. Zhang, W.Z. Fu, X.Z. Duan, X.G. Zhou, Chem. Eng. Sci. 203 (2019) 228–236.
[43] L.H. Yang, X.W. Li, Y.Y. Sun, L.H. Yue, J. Fu, X.Y. Lu, Z.Y. Hou, Catal. Commun. 101 (2017) 107–110.
[44] D. Liang, S.Y. Cui, G. Jing, J.H. Wang, P. Chen, Z.Y. Hou, Chin. J. Catal. 32 (2011) 1831–1837.
[45] D. Liang, J. Gao, J.H. Wang, P. Chen, Y.F. Wei, Z.Y. Hou, Catal. Commun. 12 (2011) 1059–1062.